Li Xiao,[1] Xuejing Zhu,[1] Shikun Yang,[1] Fuyou Liu,[1] Zhiguang Zhou,[2] Ming Zhan,[3,4] Ping Xie,[3,4] Dongshan Zhang,[1] Jun Li,[1] Panai Song,[1] Yashpal S. Kanwar,[3,4] and Lin Sun[1]

Rap1 Ameliorates Renal Tubular Injury in Diabetic Nephropathy

Rap1b ameliorates high glucose (HG)-induced mitochondrial dysfunction in tubular cells. However, its role and precise mechanism in diabetic nephropathy (DN) in vivo remain unclear. We hypothesize that Rap1 plays a protective role in tubular damage of DN by modulating primarily the mitochondria-derived oxidative stress. The role and precise mechanisms of Rap1b on mitochondrial dysfunction and of tubular cells in DN were examined in rats with streptozotocin (STZ)-induced diabetes that have Rap1b gene transfer using an ultrasound microbubble-mediated technique as well as in renal proximal epithelial tubular cell line (HK-2) exposed to HG ambiance. The results showed that Rap1b expression decreased significantly in tubules of renal biopsies from patients with DN. Overexpression of a constitutively active Rap1b G12V notably ameliorated renal tubular mitochondrial dysfunction, oxidative stress, and apoptosis in the kidneys of STZ-induced rats, which was accompanied with increased expression of transcription factor C/EBP-β and PGC-1α. Furthermore, Rap1b G12V also decreased phosphorylation of Drp-1, a key mitochondrial fission protein, while boosting the expression of genes related to mitochondrial biogenesis and antioxidants in HK-2 cells induced by HG. These effects were imitated by transfection with C/EBP-β or PGC-1α short interfering RNA. In addition, Rap1b could modulate C/EBP-β binding to the endogenous PGC-1α promoter and the interaction between PGC-1α and catalase or mitochondrial superoxide dismutase, indicating that Rap1b ameliorates tubular injury and slows the progression of DN by modulation of mitochondrial dysfunction via C/EBP-β–PGC-1α signaling.

Diabetes 2014;63:1366–1380 | DOI: 10.2337/db13-1412

COMPLICATIONS

Although glomerular injury is believed to initiate kidney damage in diabetic nephropathy (DN), recently emerging evidence suggests that tubular injury also plays a key role in the causation of damage in DN (1). Most of these studies have examined the tubular damage in the advanced stages of DN, but the mechanism(s) initiating tubular injury during this process have not been thoroughly explored.

Renal proximal tubule is uniquely susceptible to a variety of metabolic and hemodynamic factors, which is related to the events of apoptosis. Interestingly, increased apoptosis has been observed in the proximal and distal tubular epithelia in patients with diabetes (2), as well as in proximal tubular epithelial cells under high-glucose (HG) ambience (3). Thus, it is believed that the events leading to apoptosis in tubular epithelial and further progression to tubulointerstitial lesions are among the main features in DN (4). In addition, HG and angiotensin II could additively aid in the generation of reactive oxygen species (ROS), which may mediate renal

[1]Department of Nephrology, Second Xiangya Hospital, Central South University, Changsha, Hunan, China
[2]Diabetes Center, Institute of Metabolism and Endocrinology, Second Xiangya Hospital, Central South University, Changsha, Hunan, China
[3]Department of Pathology, Northwestern University, Chicago, IL
[4]Department of Medicine, Northwestern University, Chicago, IL

Corresponding author: Lin Sun, zndxsunlin11@163.com.

Received 15 September 2013 and accepted 4 December 2013.

This article contains Supplementary Data online at http://diabetes.diabetesjournals.org/lookup/suppl/doi:10.2337/db13-1412/-/DC1.

L.X. and X.Z. contributed equally to this work.

tubular cell apoptosis (5). In addition, following the uptake of glucose metabolic intermediaries via various glucose transporters, the mitochondrial electron transport system is overwhelmed in proximal tubular cells, thus causing intracellular oxidative stress and cell damage (6). Indicating that HG itself is an initiating factor may be directly responsible for the causation of tubular damage and apoptosis in DN. Nonetheless, the mechanism by which HG underpins the mitochondrial dysfunction and tubular or tubulointerstitial damage is unknown.

Rap1 is a small GTPase (7) that has been shown to regulate cell adhesion, migration, proliferation, and cell survival (8). We previously demonstrated decreased activation of Rap1b under HG ambience in vitro and found HG-induced mitochondrial dysfunction was rescued by overexpression of Rap1b in tubular cells (9). However, whether Rap1 can dampen the progression of DN in vivo by modulating mitochondrial-derived oxidative stress is unclear, and it needs to be investigated along with the delineation of the signaling pathways that may be involved.

RESEARCH DESIGN AND METHODS

Antibodies, Plasmids, and Other Reagents

Polyclonal anti-Rap1b antibody, polyclonal anti–phospho-Drp1 (Ser637) and (Ser656) antibodies, monoclonal anti–PGC-1α, and anti–C/EBP-β were from Cell Signaling Technology; human/mouse/rat cytochrome c monoclonal antibody was from BD Biosciences; procaspase-3 antibody and procaspase-9 antibody were from Thermo Fisher Scientific; monoclonal anti–cleaved caspase-3 (Asp175), rabbit polyclonal IgG antibodies including anti-mitofusin2 (Mfn2), anti-catalase, anti–manganese superoxide dismutase (Mn-SOD), anti–nuclear respiratory factor-1 (NRF-1), anti–glutathione peroxidase (GSH-Px), and anti-mtTFA were from Santa Cruz Biotechnology; and plasmids containing pcDNA/Rap1b G12V and pcDNA/Rap1b S17N mutant were generated in our laboratory as previously described (10). Extracellular signal–related kinase 1/2 (ERK1/2) short interfering RNA (siRNA), PGC-1α siRNA, DFC, MitoRed, and MitoSOX were purchased from Invitrogen.

Morphological Analysis of Kidney

Human kidney biopsy tissues were obtained from DN (N = 12) of 10–15 years' duration, and an equal number of nondiabetic patients (N = 12) were recruited for the study. The renal sections were stained with periodic acid Schiff (PAS) and periodic acid–silver methenamine (PASM). Tubulointerstitial lesion index was determined using a semiquantitative scoring system (11). Tubular damage was also scored (12), and the mitochondrial alterations in renal tubules were gauged by electron microscopy (EM) as previously described (13). The human experimental protocols as described above were approved by the Institutional Human Experimentation Ethics Committee, Second Xiangya Hospital, Central South University.

Measurements of Blood Glucose, γ-Glutamyltranspeptidase, β-*N*-Acetyl-β-D-Glucosaminidase, and Urine Albumin Excretion Levels

Blood glucose was detected by a blood glucose monitor (Boehringer Mannheim, Mannheim, Germany). The γ-glutamyltranspeptidase (γ-GT) concentrations were measured using a human γ-GT GGT ELISA kit (Biocompare), and urine β-*N*-acetyl-β-D-glucosaminidase (β-NAG) was measured by automated colorimetric method (Pacific Biomarkers, Inc.). Urine albumin was measured with a rat urine albumin ELISA kit (Bethyl Laboratories), and urine creatinine levels were tested using the QuantiChrom Creatinine Assay Kit (BioAssay Systems) following the manufacturer's protocol. Urine albumin excretion (UAE) was normalized with creatinine excretion and expressed per milligram of creatinine.

Animal Experimental Design

A total of 60 adult male Sprague-Dawley rats at 8 weeks of age (body weight 210–230 g) were divided into four groups of 15 animals each. The first group was injected with a normal saline only, which served as a control. The second group of rats received a single dose of streptozotocin (STZ; 65 mg/kg i.p.). The third group included rats with STZ-induced diabetes but injected with Rap1 V12G using ultrasound microbubble gene transfer technique (12). The fourth group included rats with STZ-induced diabetes but injected with empty vector control (STZ + empty vector). All animals were killed at 8 weeks following STZ administration. The animal experimental protocols as described above were approved by the Institutional Animal Experimentation Ethics Committee.

Ultrasound-Mediated Gene Transfer of Inducible Rap1 V12G Gene-Bearing Microbubble Into the Rat Kidneys

To control Rap1 V12G transgene expression within the kidney, a doxycycline-induced Rap1 V12G–expressing plasmid was constructed as previously described (10,14). Briefly, pTRE-Rap1b G12V was generated by subcloning a rat full-length Rap1b G12V cDNA into pTRE (Clontech, Palo Alto, CA), a tetracycline-inducible vector. An improved pTet-on vector (Clontech), pEFpurop-Tet-on, was constructed as described previously (15,16). To achieve doxycycline-inducible Rap1 G12V transgene expression in the kidney, the ultrasound microbubble-mediated system was applied as previously described (14,15). Briefly, 24 h following STZ injection, the left rat kidney was transfected with a mixture of pTR-Flag-Rap1b and pEFpurop-Tet-on with Optison (Mallinckrodt, St. Louis, MO) in 1:1 volume:volume ratio. The mixture contained 25 μg of each of the plasmids in 0.5 mL

saline, and it was introduced via the left renal artery following a temporary cessation of the renal blood supply for 3–5 min with a microclamp. Control animals received the vector without Rap1 G12V gene, and its transfection was monitored by immunohistochemistry (IHC) using a monoclonal antibody directed against Flag-M2. The Rap1b expression and activity within the kidney were assessed by quantitative real-time PCR and Western blot/immunoprecipitation, as previously described (9,10,14).

Measurements of Superoxide Generation and Apoptosis

Mitochondrial superoxide generation was detected by using a specific mitochondrial superoxide indicator, MitoSOX red (Molecular Probes). Dihydroethidium (DHE) and 5-(and 6)-chloromethyl-2′,7′-dichlorodihydrofluorescein diacetate (Wako) were used to assess the production of intracellular superoxide anion (O_2^-) and H_2O_2, respectively. The TUNEL procedure was used to gauge apoptosis following the manufacturer's instructions.

mtDNA Studies

The mtDNA damage to high- and low-molecular-weight DNA was evaluated as described previously (10,12). Briefly, PCR products were subjected to 1.6% agarose gel electrophoresis followed by staining with ethidium bromide to detect 8,636- and 316-bp DNA products. For long PCR, the primers were as follows: 5′-AGTGCA TACCGCCAAAAGA-3′ (sense) and 5′-TCTA GAGCCCACTGTAAAG-3′ (antisense). The primers for short PCR were as follows: 5′-ATGGTCTGAGCTATGA TATCAA-3′ (sense) and 5′-GATTTTGGC GTAGGTTGG-3′ (antisense).

Cellular Distribution of Phospho–Drp-1 and Mitochondrial Cytochrome c

Confocal microscopy was performed to delineate the distribution/localization of phospho–Drp-1 (p-Drp-1) as described in Wang et al. (17). The expression of Drp-1 and cytochrome c in isolated mitochondria was assessed with Western blotting procedures.

Assessment of Mitochondrial Transmembrane Potential

HK-2 cells were transfected with Rap1b, C/EBP-β–siRNA, or PGC-1α–siRNA. Then they were treated with HG, and then 10 nmol/L of TMRE dye (Molecular Probes) was added to the medium for 10 min. The mitochondrial transmembrane potential ($\Delta\psi m$) in intact cells was assessed by fluorescence-activated cell sorter (FACS) analyses and confocal microscopy using a wavelength of 582 nm. In isolated mitochondria from renal tissues, the $\Delta\psi m$ was gauged following a load of rhodamine 123 (Rh123), and $\Delta\psi m$ was calculated as discussed previously (18,19).

Mitochondrial Enzyme Activities

Mn-SOD and CuZn-SOD activity was determined using a Superoxide Dismutase Activity Assay Kit (Alexis Biochemicals). The catalase activity was measured using a Catalase Activity Colorimetric/Fluorometric Assay Kit (BioVision, Inc.), and GSH-Px was determined using the Glutathione Peroxidase Assay Kits (Biocompare, Inc.) following the manufacturers' guidelines.

Examination of Fragmentation and Length of Long Axis of Mitochondria

EM processing was used to determine mitochondrial fragmentation, and several contiguous (side-by-side) digital images were generated. The percentage of cells that had <1% long filamentous mitochondria was reflective of mitochondrial fragmentation. To determine the length of the long axis of mitochondria, digital images were generated. Then, the length of individual mitochondria in a cell was measured as described previously (13,20).

Assessment of Mitochondrial H_2O_2 Production and of Mitochondrial Permeability Transition Pore Following Ca^{2+} Load

Mitochondrial H_2O_2 production rate was evaluated using scopoletin fluorescence, as described previously (21). In addition, the mitochondrial permeability transition pore (MPTP) was evaluated by Ca^{2+} load method using a Mitochondria Calcium Fluorescence Detection Kit following the manufacturer's guidelines (Genmed Scientifics Inc.).

PGC-1α Gene Promoter Analysis

Various deletion constructs of PGC-1α promoter were generated by PCR. The PCR products were cloned into *Xho*I- and *Hind*III-digested pSEAP2-Enhancer plasmid vector (Clontech). Minimal promoter activity of the PGC-1α promoter activity was measured in the supernatants of the HK-2 using a Great EscAPe SEAP fluorescence detection kit (Clontech). The highest promoter activity was designated as being 100% like that in the studies by Irrcher et al. (22) and Sun et al. (23).

Nuclear Extract Preparation and Electrophoretic Mobility Assays

Nuclear extracts used in electrophoretic mobility assays (EMSAs) from HK-2 cells were performed as described in previous publications (24). Briefly, the nuclear extracts (10 μg) were incubated with 40,000 counts/min of [γ-^{32}P] deoxyadenosine triphosphate end-labeled oligonucleotides containing putative cAMP-response elements (CREs) within the −146 to −132 bp region of the human PGC-1α promoter corresponding to 5′-GGCTGCCTTTGAGTGACGTCA CAC-3′. The samples were then subjected to native 5% acrylamide gel electrophoresis and imaged.

Chromatin Immunoprecipitation Analysis

Chromatin immunoprecipitation (ChIP) analysis was performed using a transcription factor ChIP kit following the instruction manual (Diagenode). The primer sequences spanning −2160 to −1938 region were as follows: 5′-GGCTTCTGTTTGC CTTGCTC AG-3′ (sense) and 5′-ATACTGATACTGCGATTGTTAAG CG-3′ (antisense). This region of amplification contains forkhead box class O (FoxO1)-dependent binding element (FoxO1-DBE) in the catalase enzyme promoter. The PCR was also performed for Mn-SOD with the following sequences: 5′-GTTCCTCTTCGCCTGAC TGTT-3′ (sense) and 5′-CTGAA CCGTTTCC GTTGC TT-3′ (antisense).

RESULTS

Decreased Expression of Rap1b in Renal Tissues of Patients With DN

Morphological changes in both the glomerular and tubulointerstitial compartments, including focal tubular atrophy and interstitial fibrosis, were highlighted by PASM and PAS staining in DN patients compared with patients without DN (N-DN). IHC staining revealed a significantly decreased Rap1b expression in the renal tubules of DN patients compared with that of N-DN (Fig. 1*A*). Quantitatively, Rap1b staining intensity was decreased by >50% in renal tubules of DN patients (Fig. 1*B*). By EM, notable deformation of renal tubular mitochondria was observed in DN patients (Fig. 1*Ah*). Also, increased blood glucose and serum creatinine levels were observed in DN (Fig. 1*C* and *D*). In addition, length of the long axis of mitochondria in tubular cells of renal biopsies from patients with DN was measured, and it showed its shortening in DN compared with N-DN (Fig. 1*E*). Further analysis revealed an inverse correlation between Rap1 expression and the tubulointerstitial damage and urinary β-NAG levels (Fig. 1*F* and *G*).

Rap1b-Mediated Protective Effect on Tubular Injury in Rats With STZ-Induced Diabetes

By IHC, Rap1b expression was predominantly localized to renal proximal tubules, and it was notably decreased in renal tubules of rats with STZ-induced diabetes. However, Rap1b expression markedly increased after ultrasound-mediated gene transfer, and this was even

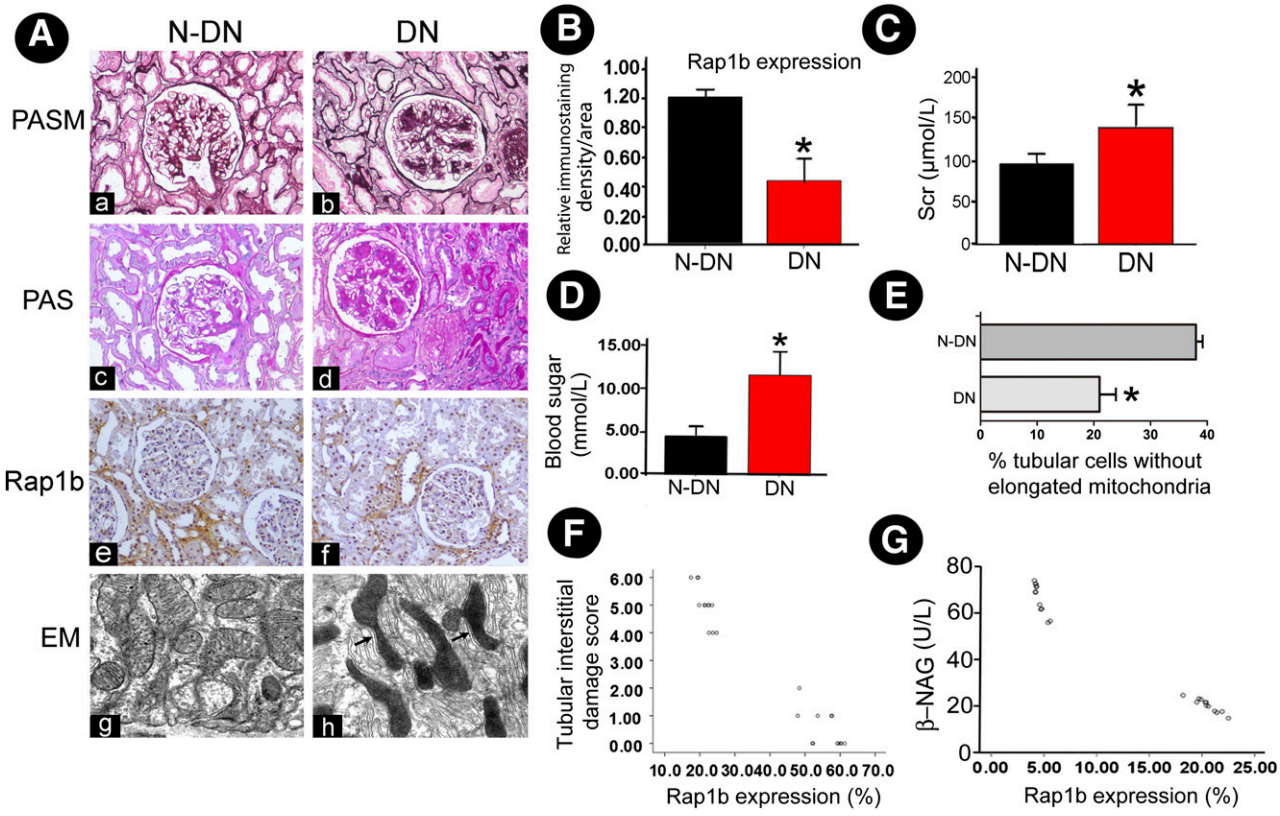

Figure 1—Decreased expression of Rap1b in renal tissues of patients with DN. *A*: PASM and PAS staining show tubular atrophy and interstitial fibrosis in renal biopsies in patients with DN (*Aa–Ad*) (magnification ×100). IHC studies revealed decreased expression of Rap1b in DN patients (*Af* vs. *Ae*). Using EM, notable deformations were seen in the tubular mitochondria of renal tissue of DN patients compared with N-DN (*Ah* vs. *Ag*) (magnification ×10,000). *B*: Averaged relative intensity following staining of anti-Rap1b antibody of kidney biopsies of DN versus N-DN patients. *$P < 0.01$. *C* and *D*: Serum creatinine (Scr) and blood glucose levels in DN and N-DN patients. *$P < 0.01$. *E*: Relative percentage of renal tubular cells with elongated mitochondria in DN versus N-DN patients. *$P < 0.01$ versus N-DN. *F* and *G*: Scatter plots show relationship between Rap1b expression and tubular interstitial damage and urinary β-NAG levels. Values are means ± SE.

much higher than constitutively expressed in control rats (Fig. 2*A*). Western blot and real-time PCR analysis revealed decreased mRNA and protein expression of Rap1b in STZ rats, while its expression was apparently high in the Rap1b G12V–treated group (Fig. 2*B–D*). Although hyperglycemia was not changed in STZ-induced diabetic rats that received Rap1b G12V (Fig. 2*E*), the rats' UAE levels were dramatically decreased following Rap1b G12V gene transfer in diabetic rats (Fig. 2*F*). The tubular damage was reflected by a significant increase in the urinary excretion of γ-GT and β-NAG in rats with STZ-induced diabetes, while they were substantially reduced by intrarenal injection of Rap1b G12V (Fig. 2*G* and *H*).

Rap1b Inhibits Renal Tubulointerstitial Fibrosis and Oxidative Stress and Apoptosis in Kidneys of Rats With STZ-Induced Diabetes

Compared with the control group, an increase in the mesangial matrix and an expansion of the tubulointerstitial compartment were observed in kidneys of rats with STZ-induced diabetes over a period of 8 weeks. These morphological alterations were ameliorated by the administration of Rap1b G12V in STZ diabetic rats. In

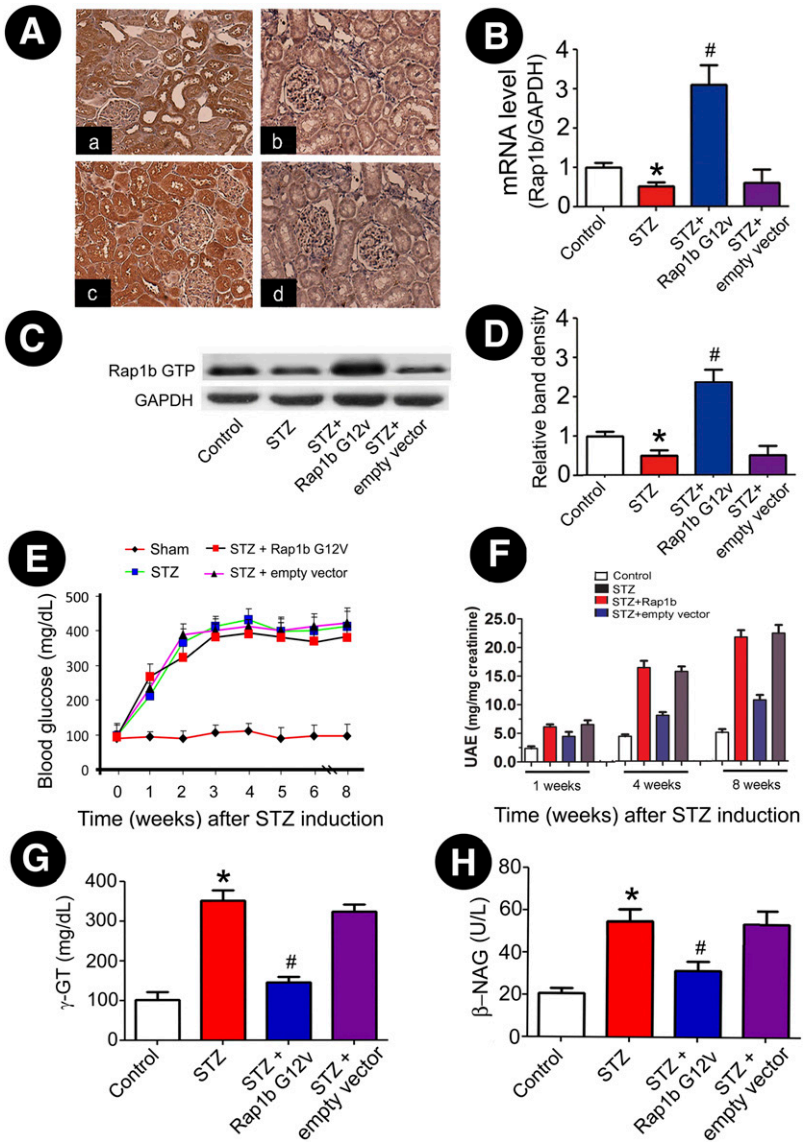

Figure 2—Expression of exogenous Rap1b in kidney tissues and its effect on blood glucose, UAE, and urinary excretion of γ-GT and β-NAG in the STZ-induced rats. *A*: Using IHC, Rap1b expression was assessed in control rats (*Aa*), STZ rats (*Ab*), STZ + Rap1b V12G rats (*Ac*), and the STZ + empty vector only group (*Ad*) (magnification ×400). Using real-time PCR (*B*) and immunoprecipitation/Western blot analyses (*C*), a decreased mRNA expression and Rap1b GTP activity was seen in kidneys of STZ rats, which was reversed by injection of Rap1b G12V. *D*: The bar graphs represent the expression of the Rap1b GTP relative to β-actin. *E*: Blood glucose concentration in each group. *F*: Rats' UAE levels. *G* and *H*: Urinary excretion of γ-GT and urine β-NAG levels. Values are means ± SE. **P* < 0.01 versus control, #*P* < 0.01 versus STZ. GAPDH, glyceraldehyde-3-phosphate dehydrogenase.

addition, there was a notable increase in collagen I (Col-1) and fibronectin (FN) expression in kidneys of diabetic rats, while it was markedly reduced following Rap1b G12V injection (Fig. 3*A–C*). These results were confirmed by Western blot analysis (Fig. 3*D–F*). In contrast, ROS production increased in renal proximal tubules of STZ rats as assessed by ROS-sensitive vital dye DHE. With overexpression of Rap1b, the ROS generation was significantly reduced. Like ROS generation, overexpression of Rap1b dramatically reduced the degree of apoptosis in cortical tubules of STZ rats by TUNEL assay with both fluorescence (TUNEL-F) and histochemical (TUNEL-H) procedures (Fig. 3*G–J*).

Overexpression of Rap1b Inhibits PGC-1α and C/EBP-β Expression and Regulation of Mitochondrial Morphologic and Functional Changes in Tubular Cells of Diabetic Rats

By suppression subtractive hybridization-PCR (SSH-PCR), PGC-1α mRNA level was notably decreased in renal tubules in STZ-induced rat kidneys compared with control subjects (figure not included). Furthermore, immunostaining showed that PGC-1α and C/EBP-β were mainly expressed in renal proximal tubules and their expression notably reduced in STZ rat kidneys compared with the control group. However, following the administration of Rap1b G12V, their expression was normalized (Fig. 4*A*). Western blot analysis confirmed the above IHC findings (Fig. 4*B–D*). In addition, marked changes in mitochondrial morphology were seen in renal tubules of STZ-induced diabetic rats. The mitochondria were often angulated and attenuated along their longitudinal axis, and some were swollen and had dilated cristae in DN rats. Moreover, frequent cristolysis with focal disruption of the inner mitochondrial membranes was observed. With Rap1b administration, the mitochondrial morphology was partially restored, and angulations and attenuation were less frequently seen (Fig. 4*E*). The length and mean area of mitochondria were also reflected by the two-dimensional EM analysis in mitochondrial fragmentation (Fig. 4*F*) along with morphometric analysis of their area (Fig. 4*G*). Since ROS formation related to the functionality of MPTP, we measured Ca^{2+} load to assess the MPTP in mitochondria isolated from renal tubules. The exposure of mitochondria to Ca^{2+} (500 μmol/L) induced a relatively increased size of MPTP opening in the STZ group compared with that of the control group. The opening was reduced to a certain extent with Rap1b G12V administration (Fig. 4*H*). In addition, a decreased mitochondrial membrane potential and increased H_2O_2 were observed in mitochondria of rat renal proximal tubules of STZ-induced diabetes, and these were reversed by Rap1b administration (Fig. 4*I* and *J*).

The expressions of procaspase-3 and procaspase-9 in the cytoplasm of tubular cells of diabetic kidneys were decreased as compared with control, but they were restored following Rap1b G12V administration. In contrast, the expression of cleaved caspase-3 was significantly increased, and it was partially blocked with the treatment of Rap1b G12V. Furthermore, the expression of mitochondrial cytochrome c (mCyto C) and p-Drp-1 increased in cytoplasm of tubular cells of diabetic kidneys, which were normalized following Rap1b G12V administration. Furthermore, the expression of mCyto C was decreased and p-Drp-1 expression increased in mitochondrial fraction from tubules in rats with STZ-induced diabetes, and both of them were normalized with Rap1b G12V administration (Supplementary Fig. 1*A–C*). Real-time PCR (Supplementary Fig. 1*D*) and Western blot analysis (Supplementary Fig. 1*E* and *F*) also revealed a notable decrease in mRNA and mitochondrial protein expression of catalase, Mn-SOD, and GSH-Px in kidneys of diabetic rats compared with control subjects. Similarly, the expression of NRF-1 and mitochondrial transcription factor A (mtTFA), which is relevant to mitochondrial biogenesis, was also decreased in kidneys of diabetic rats. Their expressions were normalized by the overexpression of Rap1 G12V. The studies were further extended to assess the relative enzyme activities of catalase, Mn-SOD, CuZn-SOD, and GSH-Px. They were also reduced in diabetic conditions, while they were normalized with the administration of Rap1 G12V (Supplementary Fig. 1*G*).

HG Inhibits Rap1 Activity in HK-2 Cells, and Overexpression of Rap1 Modulates PGC-1α Expression as Well as Regulates Mitochondrial Dysfunction via ERK1/2–C/EBP-β Pathway

Rap1b GTP activity decreased significantly in HK-2 cells exposed to HG (Supplementary Fig. 2). In addition, PGC-1α mRNA expression was notably increased in HK-2 cells transfected with Rap1bG12V by SSH-PCR (Fig. 5*A*), which was confirmed by Northern blot analysis, while overexpression of Rap1b was found to rescue HG-reduced mRNA expression of PGC-1α in HK-2 cells (Fig. 5*B*). Next, we investigated whether the Rap1b–ERK1/2–C/EBP-β signaling pathway is involved in PGC-1α modulation. By real-time PCR analysis, a dose-dependent decrease in the PGC-1α mRNA expression in HK-2 cells was observed under HG, and it was normalized by transfection of Rap1b G12V (Fig. 5*C*). The effect was partially inhibited by concomitant transfection with ERK1/2 or C/EBP-β siRNA. This effect was additive with the transfection of both siRNAs at the same time (Fig. 5*C*). Similar to mRNA, a decrease in PGC-1α protein expression was observed under HG. The effect was negated by Rap1b G12V transfection. The inhibitory effect by ERK1/2 or C/EBP-β siRNA was also reflected in HK-2 cells, as assessed by the immunofluorescence microscopy (Fig. 5*D* and *E*) and Western blot analyses (Fig. 5*F*). Furthermore, a notable decrease of C/EBP-β nuclear translocation was observed in HK-2 cells exposed to HG. With the transfection of Rap1b, the nuclear translocation of C/EBP-β was restored, while it was inhibited by ERK1/2 siRNA (Fig. 5*G* and *H*).

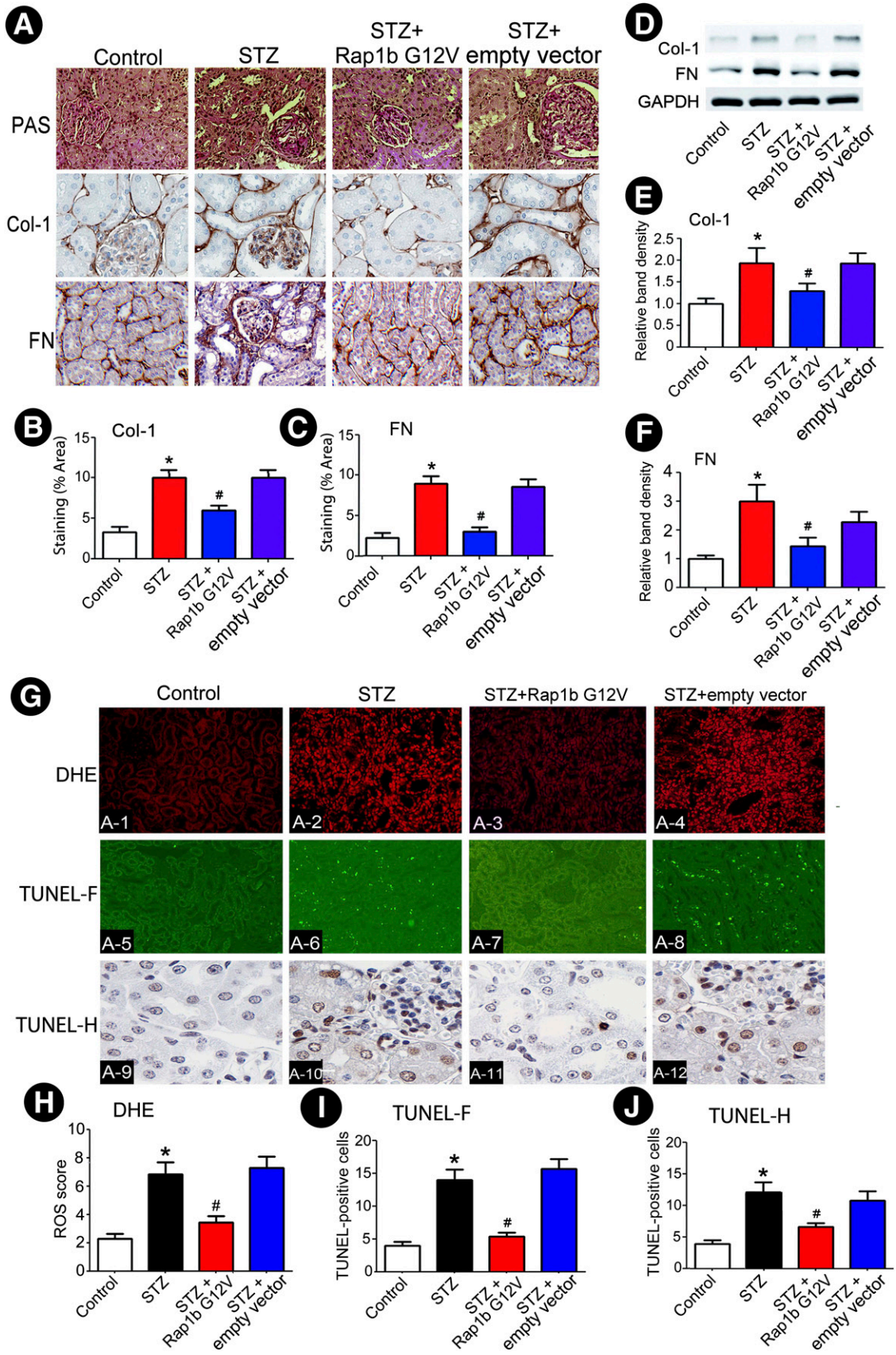

Figure 3—Effect of Rap1b G12V on renal morphology, ECM expression, oxidative stress, and apoptosis in rats kidneys with STZ-induced diabetes. *A*: Kidney sections were stained with PAS (*top* panels) and anti–Col-1 (*middle* panels) and -FN antibodies (*bottom* panels) (magnification ×400). *B* and *C*: Semiquantification of IHC staining of Col-1 and FN. *D*: Using Western blot analysis, Rap1b G12V inhibited

We also assessed whether Rap1b modulates mitochondria membrane potential ($\Delta\Psi_m$) and mtDNA fragmentation via the C/EBP-β–PGC-1α pathway in HK-2 cells subjected to HG. A loss of TMRE-associated fluorescence (indicative of $\Delta\Psi_m$) was observed in HK-2 cells subjected to HG in a time- and concentration-dependent manner. This loss was restored in cells transfected with Rap1b G12V. However, this restorative effect was partially blocked following the treatment of either C/EBP-β siRNA or PGC-1α siRNA (Supplementary Fig. 3*A*–*C*). In addition, real-time PCR showed that exposure of HK-2 cells to HG induced a dose- and time-dependent increase in mtDNA fragmentation. Transfection of Rap1b G12V partially inhibited the mtDNA damage, while C/EBP-β and/or PGC-1α siRNA blocked the protective effect of Rap1b G12V on the mtDNA damage (Supplementary Fig. 3*D* and *E*).

Rap1b Inhibits Mitochondrial ROS Production, Cytochrome c Release, and Apoptosis and Regulates the Expression and Activity of Antioxidative Genes and Phosphorylation of Drp-1 in HK-2 Cells via C/EBP-β–PGC-1a Pathway

Confocal images delineated that HG increased both mitochondrial ROS and total ROS production, while it was inhibited by overexpression of Rap1b G12V, and C/EBP-β or/and PGC-1α siRNA partially blocked the effect of Rap1b on the ROS production induced by HG in HK-2 cells (Fig. 6*A* and *B*). The FACS analysis revealed that HG caused a decreased cell survival associated with increased apoptosis, which could be reversed by overexpression of Rap1b G12V, while inhibition of C/EBP-β and/or PGC-1α by siRNA negated the Rap1b protective effect (Fig. 6*C*). In addition, HG decreased the expression of mCyto C in the mitochondrial fraction and increased its expression in the cytosolic fraction. With Rap1b transfection, its release was significantly inhibited. Accompanied with mCyto C release, procaspase-3 and procaspase-9 protein expression decreased in the cytoplasmic compartment of HK-2 cell with HG treatment. In contrast, the expression of cleaved caspase-3 was increased in the cytoplasm of HK-2 cells exposed to HG ambience. These alterations were normalized in HK-2 cells transfected with Rap1b G12V, but partially blocked with C/EBP-β or/and PGC-1α siRNA transfection (Fig. 6*D* and *E*). In addition, overexpression of Rap1 G12V in HK-2 cells ameliorated HG-induced reduction in mRNA levels of catalase, Mn-SOD, NRF-1, and mtTFA, and these effects were blocked by the pretreatment of PGC-1α and C/EBP-β siRNA. Similar changes were seen for their protein expression and ROS-scavenging enzyme activity (Supplementary Fig. 4).

In addition, HG ambience increased the p-Drp-1 at Ser637 in HK-2 cells, while this effect was abolished by Rap1b G12V transfection (Fig. 6*F*). However, transfection with Rap1b mutant construct (Rap1b S17N) failed to inhibit p-Drp-1 expression in HK-2 cells under HG. Associated with the change in p-Drp-1 expression, the mitochondria became relatively more fragmented in a time-dependent manner under HG, and this process could be inhibited by overexpression of Rap1b G12V (Fig. 6*G*). Moreover, increasing frequency of cells undergoing apoptosis in a time-dependent manner induced by HG was found, as assessed by cytometric analysis. The extent of cells undergoing apoptosis was reduced by overexpression of Rap1b G12V (Fig. 6*H*). Western blot analyses indicated an imbalance induced by HG between fusion and fission events of mitochondria, as reflected by increasing the protein expression of p-Drp-1 and decreasing expression of Mfn2, and these changes were reversed with the overexpression of Rap1b but not with Rap1b S17N mutant transfection. Interestingly, ERK1/2 siRNA could also partially block the normalizing effect of Rap1b G12V (Fig. 6*I*).

Modulation of PGC-1α Promoter Activity by Rap1b

A ~2.0-kb fragment upstream of open reading frame of human PGC-1α was isolated and cloned into pSEAP-1. Five deletion constructs spanning different regions of PGC-1α promoter were generated and subcloned into pSEAP1-enhancer vector. The highest SEAP activity was observed in the deletion construct spanning +28 to −1136 bp upstream of the open reading frame (Fig. 7*A*). This construct was used for the subsequent experiments. HG ambience inhibited the activity of PGC-1α promoter in a dose-dependent manner (Fig. 7*B*). Transfection of Rap1b G12V restored activity of PGC-1α promoter under HG, almost close to basal conditions. This restorative effect was partially abolished with the concomitant transfection of ERK1/2 or C/EBP-β siRNA (Fig. 7*C*), suggesting that the protective effect of Rap1b on the HG inhibition of PGC-1α promoter activity is dependent upon the ERK1/2–C/EBP-β pathway.

To verify whether Rap1 regulation of PGC-1α promoter activity is related to binding of transcription factor C/EBP-β to PGC-1α DNA, EMSA was carried out. The binding of the C/EBP-β oligonucleotide was noted to be reduced in the nuclear extracts from HK-2 cells subjected to HG. However, transfection of Rap1b G12V could

the expression of Col-1 and FN in rats with STZ-induced diabetes. *E* and *F*: Quantification of average band density calculated from different Western blots. *G*: Increased oxidative stress and apoptosis was seen in tubular cells of diabetic rat kidneys, as assessed by DHE (*top* panels) and TUNEL-F (*middle* panels) or -H (*bottom* panels) staining, while the effect was reduced by transfection of Rap1b G12V plasmid into the kidney. *H*–*J*: Quantification of tissues stained with DHE, TUNEL-F, and TUNEL-H procedures. Values are means ± SE. **P* < 0.01 versus control; #*P* < 0.01 versus STZ. *N* = 6. GAPDH, glyceraldehyde-3-phosphate dehydrogenase.

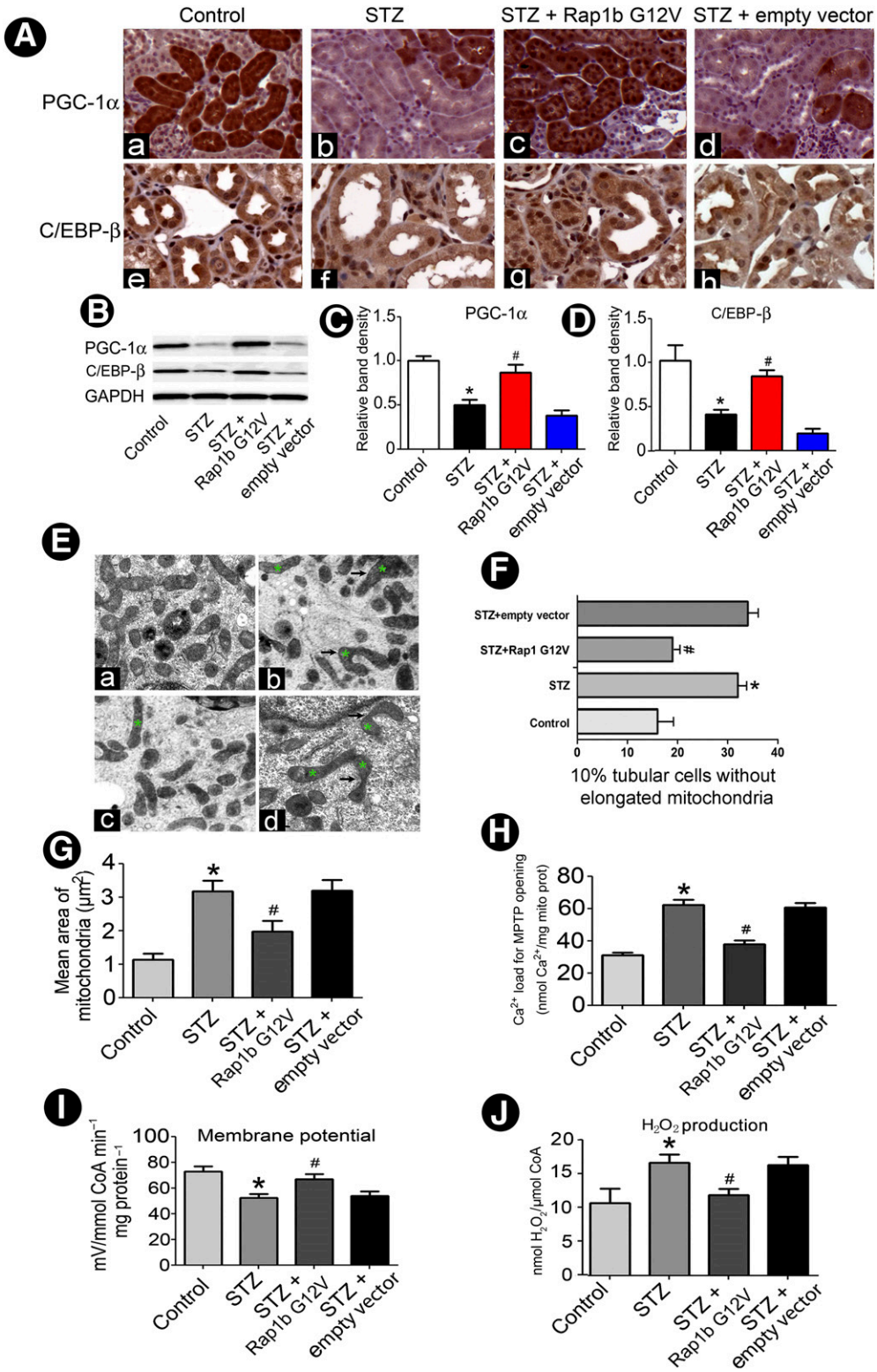

Figure 4—Effect of overexpression Rap1b on PGC-1α and C/EBP-β protein expression and the hyperglycemia-induced altered mitochondrial morphology and function in diabetic rat kidneys. *A*: IHC studies revealed a decreased in situ expression of both PGC-1α (*top* panels) and C/EBP-β (*bottom* panels) in the respective cytoplasmic and nuclear compartments of renal tubules in kidneys of rats with STZ-induced diabetes. Similar expression patterns were seen using Western blotting analyses (*B*). *C* and *D*: Quantification of average band intensity of Western blots. *E*: Using EM, deformation of mitochondria with dilatation of the cristae was seen in kidneys of rats with STZ-induced diabetes; (*Eb*) versus control (*Ea*). With Rap1b overexpression, aberrant cristae was reduced, but residual swelling of mitochondria was seen; (*Ec*) versus STZ + empty vector (*Ed*). Asterisks represent the deformations of mitochondria. *F*: Relative percentage of tubules with elongated mitochondria in DN versus N-DN rats and following Rap1b transfection. *G*: Bar graphs depict mitochondrial area per square micrometer in tubular cells of the kidney in four groups. Ca^{2+}-induced MPTP opening (*H*), mitochondrial membrane potential (*I*), and H_2O_2 production (*J*). Values are means ± SE. **P* < 0.01 versus control; #*P* < 0.01 versus STZ groups. GAPDH, glyceraldehyde-3-phosphate dehydrogenase; mito prot, mitochondrial protein.

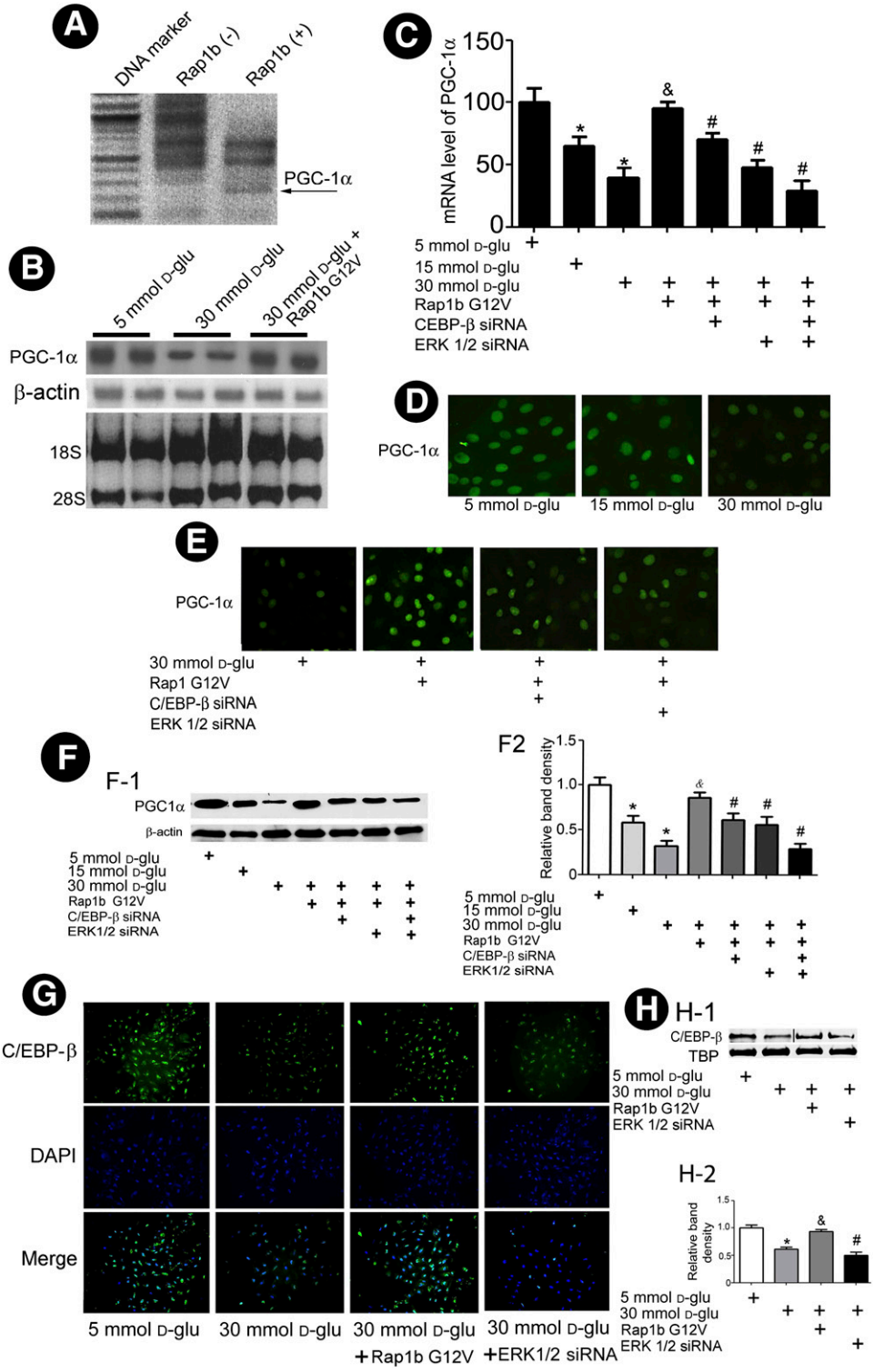

Figure 5—Effect of Rap1b on PGC-1α and C/EBP-β nuclear translocation in HK-2 cells under HG ambience. *A*: SSH-PCR shows upregulated expression of PGC-1α mRNA (arrow) in HK-2 cells transfected with Rap1 G12V. Northern blot analyses (*B*) and real-time PCR analyses (*C*) showed overexpression of Rap1 G12V reversed the HG-induced reduction in PGC-1α mRNA expression, while pretreatment of HK-2 cells with ERK1/2 siRNA or C/EBP-β siRNA negated this reversal effect. *D*: Photomicrographs showing that HG decreases nuclear translocation of PGC-1α, while overexpression of Rap1b G12V normalized the nuclear translocation. *E*: Prior treatment of HK-2 cells with C/EBP-β or ERK1/2 siRNA partially negated the Rap1b G12V–related restorative effect. *F-1*: Western blot analysis showed PGC-1α expression of nuclear protein in HK-2 cells. *F-2*: Quantification of average band intensity from four separate Western blots. *G*: Cellular immunofluorescence showing that overexpression of Rap1b G12V blocks the HG-induced inhibition of nuclear translocation of C/EBP-β in HK-2 cells, while the effect was abolished in cells transfected with ERK1/2 siRNA. These results were confirmed by Western blot analysis; TATA-binding protein (TBP) as nuclear protein loading control (*H-1* and *H-2*). Bar graph represents the quantification of average band intensity. Values are means ± SE. *$P < 0.01$ vs. 5 mmol/L D-glucose (D-glu); &$P < 0.01$ vs. 30 mmol/L D-glucose; #$P < 0.01$ vs. 30 mmol/L D-glucose + Rap1b.

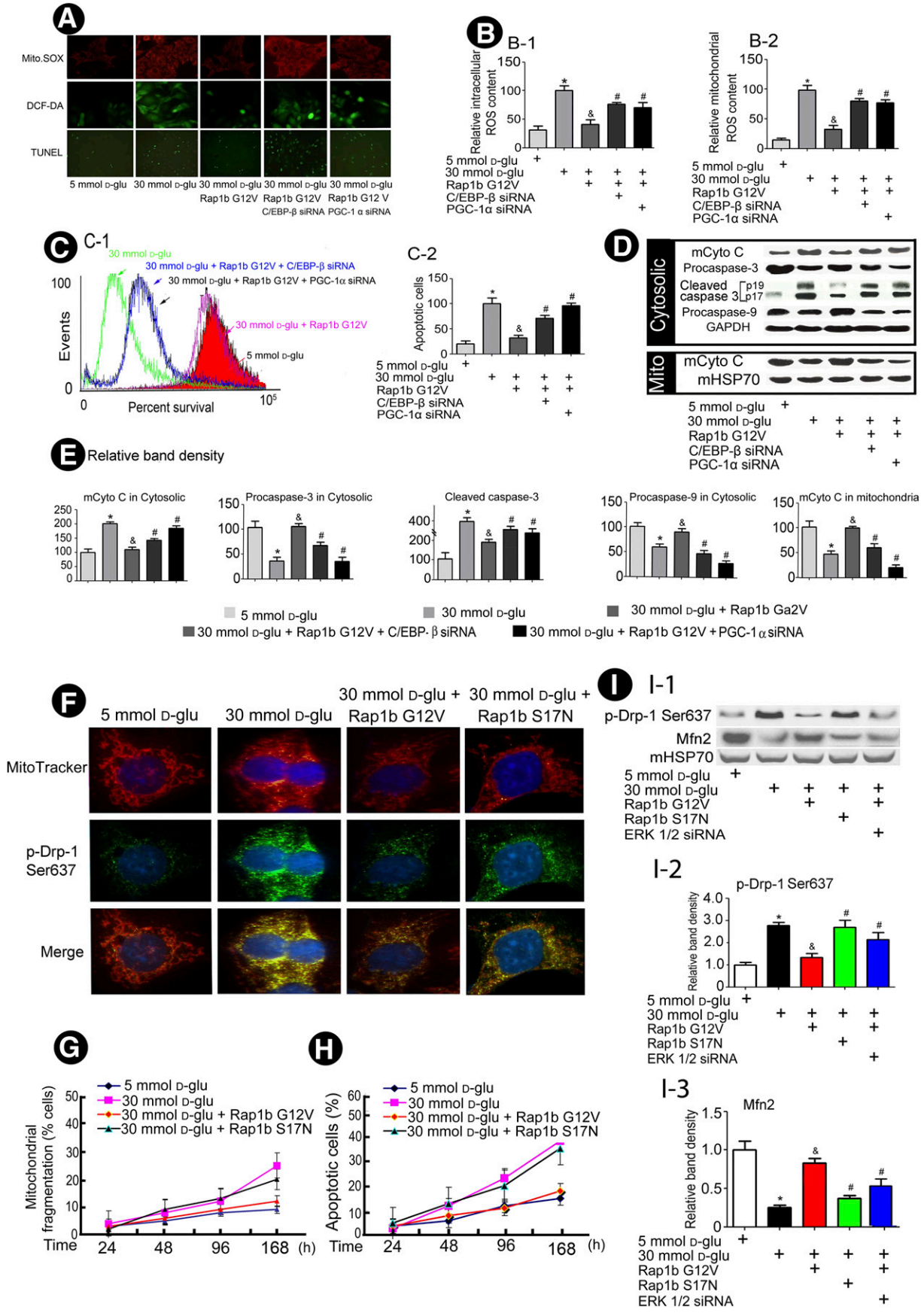

Figure 6—Overexpression of Rap1b inhibits generation of ROS and mCyto C release from mitochondria and decreases apoptotic protein expression and mitochondrial altered dynamics in HK-2 cells induced by HG. *A*: Confocal images reveal the levels of mitochondrial ROS

partially normalize the band density, while it was reduced in cells treated with C/EBP-β siRNA. The super shift observed by the use of anti–PGC-1α antibody confirmed the specificity of EMSA experiments (Fig. 7*D*).

We also used ChIP assay coupled with PCR to determine the interaction of PGC-1α with the catalase or Mn-SOD promoter region in HK-2 cells. These results support the notion that the PGC-1α could physically interact with the potential binding sites of FoxO1-DBE in catalase or Mn-SOD promoters. The band densities of PCR products remarkably decreased following treatment with HG. Mannitol had no effect. The overexpression of Rap1b G12V restored the band density to basal levels (Fig. 7*E*), while they remained reduced as seen in that of HG with the transfection of Rap1b S17N mutant or cotransfected with Rap1b G12V and C/EBP-β siRNA (Fig. 7*F*).

DISCUSSION

It is known that substitution of glycine at residue 12 to valine (GGC → GTC) alters the GTPase activity (25). This results in constitutive activation of Rap1b to enhance the mitogenic response mediated by cAMP while maintaining cellular differentiation (26). Thus, the Rap1b G12V mutant construct was used in this study to delineate its effect in regulation of tubular injury in diabetic state. To modulate and overexpress Rap1 G12V transgene inducible expression within the kidney, a doxycycline-induced Rap1 G12V–expressing plasmid was constructed using the Tet-On system. The ultrasound microbubble-mediated transgene method was used for the delivery of these plasmids. The ultrasound microbubble-mediated transgene method is a novel, nonviral, effective, and safe method for delivering drugs or genes to target organs or cells (14). This technique has been used to observe the role of Smad7 in STZ-induced DN for 5 weeks (27). In this study, we used this procedure to transfer Rap1b G12V gene into the rat kidney, and then kidneys were harvested and used for IHC and Northern and Western blot analysis. We found that overexpression of Rap1b G12V could reverse the changes in renal tissues induced by hyperglycemia and rectify the UAE, γ-GT, and β-NAG and decreased the expression of Col-1 and FN in the kidneys of STZ-induced rats (Figs. 3 and 4), suggesting that Rap1b G12V exerts a beneficial effect in tubular injury in DN. The pathogenesis of DN is multifactorial, the dominant being ROS-mediated injury.

Mitochondrial dysfunction could be a contributing factor to the pathogenesis and complication of diabetes mellitus (28). The mitochondrial-mediated pathway leading to apoptosis is one of the most important cell death signaling pathways that cause release of mCyto C and activation of caspases-9 and -3, leading ultimately to apoptosis (29). Interestingly, transient transfection of constitutively active Rap1 G12V into C2C12 myotubes leads to a partial rescue of simvastatin-induced inhibition of mitochondrial respiration (30). In this study, we observed that overexpression of Rap1b G12V could reverse ROS generation and apoptosis by protecting mitochondrial dysfunction in the renal proximal tubules of diabetic rats and in cultured tubular cells induced by HG.

PGC-1α may exert a rescuing effect in preserving the mitochondrial function and maintaining homeostasis of oxidative metabolism (31). Its expression seems to be regulated by C/EBP-β, a cAMP-regulated transcription factor (32). Decreased PGC-1α expression in muscle tissues of patients with patients with diabetes may be responsible for decreased expression of NRF-dependent metabolic and mitochondrial genes (33). Furthermore, the PKA plays a critical role in the regulation of PGC-1α expression (34), and ERK1/2 activation is essential for cAMP-dependent C/EBP-β activation, which can phosphorylate and activate C/EBP-β (35). In this study, we demonstrate that overexpression or overactivity of Rap1b could upregulate HG-induced reduction of PGC-1α mRNA and protein expression, while reducing its nuclear translocation by ERK1/2 or C/EBP-β siRNA pathway in the kidneys of STZ rats and HK-2 cells induced by HG.

PGC-1α is also a master regulator of ROS-scavenging enzymes including Mn-SOD2, catalase, GSH-Px, and uncoupling protein 2 (36). Reduction of PGC-1α expression may promote oxidative stress (37). In this study, activation of Rap1 regulates mitochondrial ROS production by increasing antioxidative enzyme gene expression modulation via the ERK1/2, C/EBP-β, and PGC-1α signaling pathway in the kidneys of diabetic animals. In addition, PGC-1α has a major impact on regulation of mitochondrial DNA replication and inducing gene expression for NRF-1, NRF-2, and mtTFA by interacting with NRF-1 and thereby coactivating its transcriptional activity (38). NRF-1 may regulate nuclear genes encoding respiratory subunits and components of mitochondrial transcriptional and replication machinery (39). We also

and intracellular ROS in HK-2 cells. *B*: The bar graphs represent a summary of FACS experiments of MitoSOX (*B-1*) or DFC (*B-2*) studies. *C*: FACS analyses depict cell survival (*C-1*), the bar graph represents a summary of FACS experiment from FITC Annexin V studies (*C-2*). *D*: Western blots of cytosolic proteins show an altered expression of mCyto C and cleaved caspase-3 and procaspase-3 and -9. *E*: The bar graphs represent the quantification of average band intensity of *D*. *F*: Confocal microscopy of HK-2 cells stained with MitoTracker (red) and anti-p-Drp (Ser637) antibody (green). *G*: Mitochondrial fragmentation in HK-2 cells treated with 5 and 30 mmol/L D-glucose for 24–168 h. *H*: Flow cytometric analyses with FITC Annexin V staining. *I*: Western blot analyses (*I-1*) of mitochondrial extract from HK-2 cells and bar graphs (*I-2* and *I-3*) represent the band intensity. Values are means ± SE. **P* < 0.01 vs. 5 mmol/L D-glucose (D-glu); &*P* < 0.01 vs. 30 mmol/L D-glucose; #*P* < 0.01 vs. 30 mmol/L D-glucose + Rap1b. Mito, mitochondria.

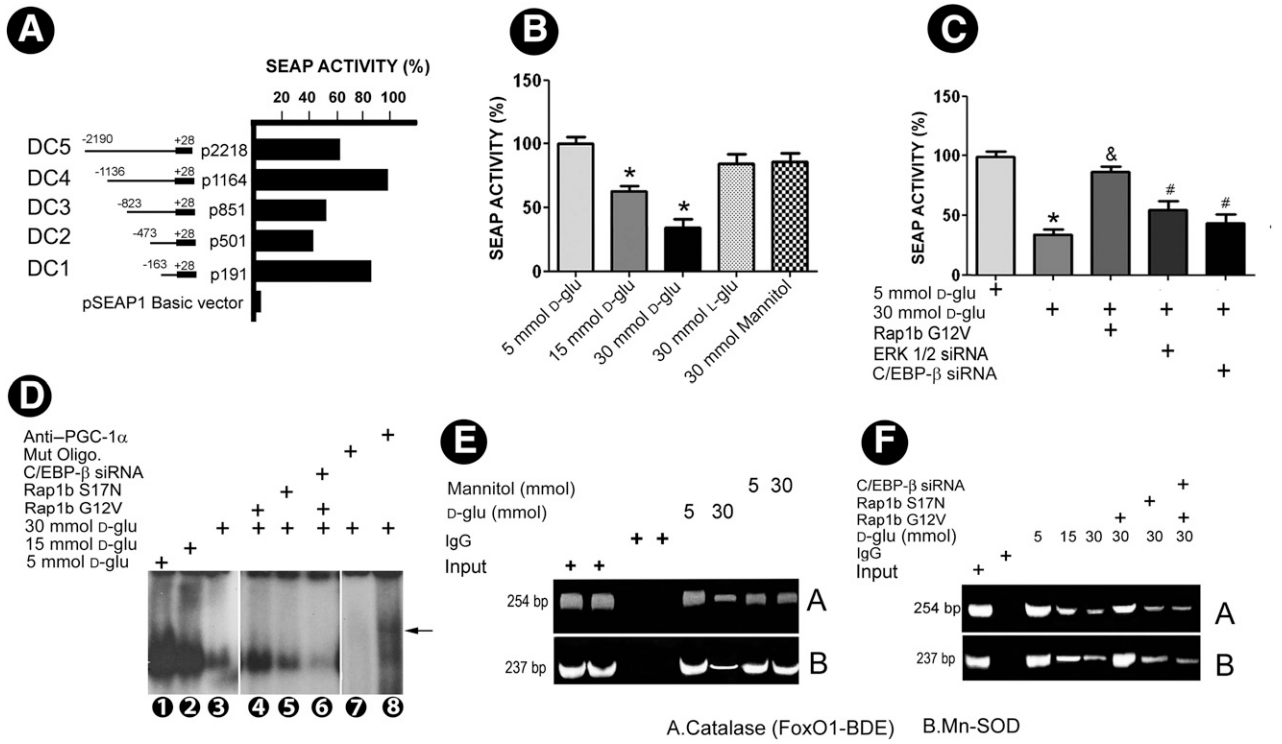

Figure 7—Effect of Rap1b on PGC-1α promoter activity, C/EBP-β binding to PGC-1α promoter, and interaction between PGC-1α promoter with promoters of catalase and Mn-SOD. *A*: Five deletion constructs (DC1–5) spanning different regions of PGC-1α promoter subcloned into pSEAP1-enhancer vector and their respective activities. *B*: Promoter analysis in DC4 construct following various treatments. *C*: Transfection of Rap1b G12V plasmid individually led to a 40–50% increase in the SEAP activity under HG ambience, while blocked partially with the cotransfection of ERK 1/2 siRNA or PGC-1α siRNA. *D*: EMSAs show C/EBP-β binding in human PGC-1α promoter in samples isolated from nuclear extracts of HK-2 cells subjected to HG, while a significant reversal in the band intensity was seen following transfection with Rap1b G12V construct. The reversal effect was not seen following transfection of Rap1b S17G mutant or C/EBP-β siRNA. *E*: ChIP assay yielded 254-bp (catalase) and 237-bp (Mn-SOD) products with decreased band intensity in anti–PGC-1α antibody immunoprecipitated nuclear material from cells subjected HG compared with that of 5 mmol/L glucose. The decreased intensity was restored in cells transfected with Rap1b G12V, while this effect was abolished with the transfection of Rap1b S17G mutant or C/EBP-β siRNA (*F*). Values are means ± SEM. $N = 4$. *$P < 0.05$ vs. 5 mmol/L D-glucose; $$P < 0.01$ vs. 30 mmol/L D-glucose; #$P < 0.05$ vs. 30 mmol/L + Rap1b G12V. IgG, immunoglobulin G; Mut Oligo, mutated oligonucleotide.

noted that overexpression of Rap1b could also regulate the gene and protein expression of mtTFA and NFR-1 in diabetic kidney tissues via C/EBP-β–PGC-1α signaling.

A perturbation in the balance between mitochondrial fission proteins Drp-1/DLP1/Dnm1 and mitochondrial inner membrane fusion protein Mfn2 leads to mitochondrial fragmentation (40). Under HG ambience, the mitochondria are relatively small, compact with decreased expression of Mfn1, while they increase in Drp1 (41), which is likely to lead to mitochondrial and cellular dysfunction (42). In addition, ERK is believed to be one of the intracellular regulators of signaling for Drp-1 (43), and Rap1b is known to play a role in cell adhesion, migration, and tubule formation by coupling to ERK (44). In this study, we observed that Rap1 regulates mitochondrial dysfunction induced by HG via the inhibition of phosphorylation of Drp1 dependent on the ERK 1/2 signaling pathway.

It is known that C/EBP-β binds to CREs in the PGC-1α promoter at −756 to −752 bp, which is essential for PGC-1α activation (22). In this study, we also demonstrated that Rap1b G12V could reverse HG-reduced binding with C/EBP-β at the CRE site of the PGC-1α promoter. In contrast, FoxO1 has been described to protect pancreatic β-cells against oxidative stress–induced dysfunction (45). PGC-1α can interact with the regulatory promoter sequences of Mn-SOD and catalase through FoxO1 (46). To further investigate whether Rap1 regulates expression of oxidative stress–protective genes, ChIP experiments were performed. PGC-1α binding to catalase and Mn-SOD promoter at FoxO1-DBE sites was reduced under HG ambience in HK-2 cells, while overexpression of Rap1 could reverse this effect via C/EBP signaling.

In conclusion, it seems that hyperglycemia inhibits Rap1 expression and its activity. This leads to tubular cell injury in patients with DN and STZ-induced diabetic animal models. This mechanism involves a decreased PGC-1α expression via the ERK1/2–C/EBP-β pathway and phosphorylation of Drp-1, thus inducing an imbalance between mitochondrial fission and fusion proteins, which is followed by a series of events leading to

overproduction of ROS and tubular apoptosis (Supplementary Fig. 5). These events are reversed with the overexpression of Rap1b, suggesting activation of Rap1b could decelerate the progression of DN by regulation of mitochondrial dysfunction via the ERK-C/EBP-β–PGC-1α signaling pathway.

Funding. This work was supported by grants from the Creative Research Group Fund of the National Foundation Committee of Natural Sciences of China (30971379, 81270812, and 81370832), the Doctoral Fund of Ministry of Education of China (20110162110012), the Furong Scholars Fund from Hunan Province Education Department, National Basic Research Program of China 973 (2012CB517601), Program for Changjiang Scholars and Innovative Research Team in University (IRT1195), and a grant from the National Institutes of Health (DK-60635).

Duality of Interest. No potential conflicts of interest relevant to this article were reported.

Author Contributions. L.X. and X.Z. generated the data for the manuscript and partially wrote the manuscript. S.Y., D.Z., J.L., and P.S. generated the data for the manuscript. F.L., Z.Z., M.Z., and P.X. discussed the results of the manuscript. Y.S.K. and L.S. edited the manuscript. L.S. is the guarantor of this work and, as such, had full access to all the data in the study and takes responsibility for the integrity of the data and the accuracy of the data analysis.

References

1. Magri CJ, Fava S. The role of tubular injury in diabetic nephropathy. Eur J Intern Med 2009;20:551–555
2. Kumar D, Robertson S, Burns KD. Evidence of apoptosis in human diabetic kidney. Mol Cell Biochem 2004;259:67–70
3. Sun L, Xiao L, Nie J, et al. p66Shc mediates high-glucose and angiotensin II-induced oxidative stress renal tubular injury via mitochondrial-dependent apoptotic pathway. Am J Physiol Renal Physiol 2010;299: F1014–F1025
4. Habib SL. Diabetes and renal tubular cell apoptosis. World J Diabetes 2013;4:27–30
5. Kanwar YS, Sun L, Xie P, Liu FY, Chen S. A glimpse of various pathogenetic mechanisms of diabetic nephropathy. Annu Rev Pathol 2011;6:395–423
6. Kanwar YS, Wada J, Sun L, et al. Diabetic nephropathy: mechanisms of renal disease progression. Exp Biol Med (Maywood) 2008;233:4–11
7. Fischer TH, Gatling MN, Lacal JC, White GC 2nd. rap1B, a cAMP-dependent protein kinase substrate, associates with the platelet cytoskeleton. J Biol Chem 1990;265:19405–19408
8. Dubé N, Kooistra MR, Pannekoek WJ, et al. The RapGEF PDZ-GEF2 is required for maturation of cell-cell junctions. Cell Signal 2008;20:1608–1615
9. Sun L, Xie P, Wada J, et al. Rap1b GTPase ameliorates glucose-induced mitochondrial dysfunction. J Am Soc Nephrol 2008;19:2293–2301
10. Lin S, Sahai A, Chugh SS, et al. High glucose stimulates synthesis of fibronectin via a novel protein kinase C, Rap1b, and B-Raf signaling pathway. J Biol Chem 2002;277:41725–41735
11. Zhang Z, Sun L, Wang Y, et al. Renoprotective role of the vitamin D receptor in diabetic nephropathy. Kidney Int 2008;73:163–171
12. Haruna Y, Kashihara N, Satoh M, et al. Amelioration of progressive renal injury by genetic manipulation of Klotho gene. Proc Natl Acad Sci U S A 2007;104:2331–2336
13. Brooks C, Wei Q, Cho SG, Dong Z. Regulation of mitochondrial dynamics in acute kidney injury in cell culture and rodent models. J Clin Invest 2009; 119:1275–1285
14. Lan HY, Mu W, Tomita N, et al. Inhibition of renal fibrosis by gene transfer of inducible Smad7 using ultrasound-microbubble system in rat UUO model. J Am Soc Nephrol 2003;14:1535–1548
15. Zhong X, Chung AC, Chen HY, Meng XM, Lan HY. Smad3-mediated upregulation of miR-21 promotes renal fibrosis. J Am Soc Nephrol 2011;22: 1668–1681
16. Mizushima S, Nagata S. pEF-BOS, a powerful mammalian expression vector. Nucleic Acids Res 1990;18:5322
17. Wang W, Wang Y, Long J, et al. Mitochondrial fission triggered by hyperglycemia is mediated by ROCK1 activation in podocytes and endothelial cells. Cell Metab 2012;15:186–200
18. Emaus RK, Grunwald R, Lemasters JJ. Rhodamine 123 as a probe of transmembrane potential in isolated rat-liver mitochondria: spectral and metabolic properties. Biochim Biophys Acta 1986;850: 436–448
19. de Cavanagh EM, Toblli JE, Ferder L, Piotrkowski B, Stella I, Inserra F. Renal mitochondrial dysfunction in spontaneously hypertensive rats is attenuated by losartan but not by amlodipine. Am J Physiol Regul Integr Comp Physiol 2006;290:R1616–R1625
20. Song R, Bian H, Wang X, Huang X, Zhao KS. Mitochondrial injury underlies hyporeactivity of arterial smooth muscle in severe shock. Am J Hypertens 2011;24:45–51
21. Piotrkowski B, Fraga CG, de Cavanagh EM. Mitochondrial function and nitric oxide metabolism are modified by enalapril treatment in rat kidney. Am J Physiol Regul Integr Comp Physiol 2007;292:R1494–R1501
22. Irrcher I, Ljubicic V, Kirwan AF, Hood DA. AMP-activated protein kinase-regulated activation of the PGC-1alpha promoter in skeletal muscle cells. PLoS ONE 2008;3:e3614
23. Sun L, Kondeti VK, Xie P, Raparia K, Kanwar YS. Epac1-mediated, high glucose-induced renal proximal tubular cells hypertrophy via the Akt/p21 pathway. Am J Pathol 2011;179:1706–1718
24. Wang H, Peiris TH, Mowery A, Le Lay J, Gao Y, Greenbaum LE. CCAAT/enhancer binding protein-beta is a transcriptional regulator of peroxisome-proliferator-activated receptor-gamma coactivator-1alpha in the regenerating liver. Mol Endocrinol 2008;22:1596–1605
25. Ribeiro-Neto F, Urbani J, Lemee N, Lou L, Altschuler DL. On the mitogenic properties of Rap1b: cAMP-induced G(1)/S entry requires activated and phosphorylated Rap1b. Proc Natl Acad Sci USA 2002;99: 5418–5423
26. Edreira MM, Li S, Hochbaum D, et al. Phosphorylation-induced conformational changes in Rap1b: allosteric effects on switch domains and effector loop. J Biol Chem 2009;284:27480–27486
27. Chen HY, Huang XR, Wang W, et al. The protective role of Smad7 in diabetic kidney disease: mechanism and therapeutic potential. Diabetes 2011;60:590–601
28. Wallace DC. A mitochondrial paradigm of metabolic and degenerative diseases, aging, and cancer: a dawn for evolutionary medicine. Annu Rev Genet 2005;39:359–407
29. Yang JC, Cortopassi GA. Induction of the mitochondrial permeability transition causes release of the apoptogenic factor cytochrome c. Free Radic Biol Med 1998;24:624–631
30. Mullen PJ, Zahno A, Lindinger P, et al. Susceptibility to simvastatin-induced toxicity is partly determined by mitochondrial respiration and phosphorylation state of Akt. Biochim Biophys Acta 2011;1813:2079–2087

31. Mitra R, Nogee DP, Zechner JF, et al. The transcriptional coactivators, PGC-1α and β, cooperate to maintain cardiac mitochondrial function during the early stages of insulin resistance. J Mol Cell Cardiol 2012;52:701–710
32. Than TA, Lou H, Ji C, Win S, Kaplowitz N. Role of cAMP-responsive element-binding protein (CREB)-regulated transcription coactivator 3 (CRTC3) in the initiation of mitochondrial biogenesis and stress response in liver cells. J Biol Chem 2011;286:22047–22054
33. Patti ME, Butte AJ, Crunkhorn S, et al. Coordinated reduction of genes of oxidative metabolism in humans with insulin resistance and diabetes: Potential role of PGC1 and NRF1. Proc Natl Acad Sci U S A 2003;100:8466–8471
34. Sheng B, Wang X, Su B, et al. Impaired mitochondrial biogenesis contributes to mitochondrial dysfunction in Alzheimer's disease. J Neurochem 2012;120:419–429
35. Borland G, Bird RJ, Palmer TM, Yarwood SJ. Activation of protein kinase Calpha by EPAC1 is required for the ERK- and CCAAT/enhancer-binding protein beta-dependent induction of the SOCS-3 gene by cyclic AMP in COS1 cells. J Biol Chem 2009;284:17391–17403
36. Chen SD, Yang DI, Lin TK, Shaw FZ, Liou CW, Chuang YC. Roles of Oxidative Stress, Apoptosis, PGC-1α and Mitochondrial Biogenesis in Cerebral Ischemia. Int J Mol Sci 2011;12:7199–7215
37. Coll T, Jové M, Rodríguez-Calvo R, et al. Palmitate-mediated downregulation of peroxisome proliferator-activated receptor-gamma coactivator 1alpha in skeletal muscle cells involves MEK1/2 and nuclear factor-kappaB activation. Diabetes 2006;55:2779–2787
38. Klinge CM. Estrogenic control of mitochondrial function and biogenesis. J Cell Biochem 2008;105:1342–1351
39. Campbell CT, Kolesar JE, Kaufman BA. Mitochondrial transcription factor A regulates mitochondrial transcription initiation, DNA packaging, and genome copy number. Biochim Biophys Acta 2012;1819:921–929
40. Galloway CA, Yoon Y. Mitochondrial morphology in metabolic diseases. Antioxid Redox Signal 2013;19:415–430
41. Gao CL, Zhu C, Zhao YP, et al. Mitochondrial dysfunction is induced by high levels of glucose and free fatty acids in 3T3-L1 adipocytes. Mol Cell Endocrinol 2010;320:25–33
42. Youle RJ, Karbowski M. Mitochondrial fission in apoptosis. Nat Rev Mol Cell Biol 2005;6:657–663
43. Baixauli F, Martín-Cófreces NB, Morlino G, et al. The mitochondrial fission factor dynamin-related protein 1 modulates T-cell receptor signalling at the immune synapse. EMBO J 2011;30:1238–1250
44. Bouschet T, Perez V, Fernandez C, Bockaert J, Eychene A, Journot L. Stimulation of the ERK pathway by GTP-loaded Rap1 requires the concomitant activation of Ras, protein kinase C, and protein kinase A in neuronal cells. J Biol Chem 2003;278:4778–4785
45. Kitamura YI, Kitamura T, Kruse JP, et al. FoxO1 protects against pancreatic beta cell failure through NeuroD and MafA induction. Cell Metab 2005;2:153–163
46. Xiong S, Salazar G, San Martin A, et al. PGC-1 alpha serine 570 phosphorylation and GCN5-mediated acetylation by angiotensin II drive catalase down-regulation and vascular hypertrophy. J Biol Chem 2010;285:2474–2487